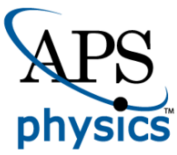

X-ray Echo Spectroscopy

Yuri Shvyd'ko

Phys. Rev. Lett. **116**, 080801 — Published 25 February 2016

DOI: 10.1103/PhysRevLett.116.080801

X-ray echo spectroscopy

Yuri Shvyd'ko[1,*]

[1] *Advanced Photon Source, Argonne National Laboratory, Argonne, Illinois 60439, USA*

X-ray echo spectroscopy, a counterpart of neutron spin-echo, is being introduced here to overcome limitations in spectral resolution and weak signals of the traditional inelastic x-ray scattering (IXS) probes. An image of a point-like x-ray source is defocused by a dispersing system comprised of asymmetrically cut specially arranged Bragg diffracting crystals. The defocused image is refocused into a point (echo) in a time-reversal dispersing system. If the defocused beam is inelastically scattered from a sample, the echo signal acquires a spatial distribution, which is a map of the inelastic scattering spectrum. The spectral resolution of the echo spectroscopy does not rely on the monochromaticity of the x-rays, ensuring strong signals along with a very high spectral resolution. Particular schemes of x-ray echo spectrometers for 0.1–0.02-meV ultra-high-resolution IXS applications (resolving power $> 10^8$) with broadband $\simeq$ 5–13 meV dispersing systems are introduced featuring more than 10^3 signal enhancement. The technique is general, applicable in different photon frequency domains.

PACS numbers: 07.85.Nc, 41.50.+h, 78.70.Ck, 07.85.Fv

The spectroscopic signal strength decreases abruptly with improving spectral resolution. An x-ray echo spectroscopy, introduced here, offers a potential for achieving much higher, yet unattainable, spectral resolution in the hard x-ray regime without compromising the signal strength.

The origin of the proposed technique is in spin echo, a phenomenon discovered by Erwin Hahn in 1950 [1]. Spin echo is the refocusing in the time domain of the defocused spin magnetization by time reversal. The spin echo technique is widely used in NMR. There is a photon echo analog in the optics. Neutron spin echo spectroscopy is an inelastic neutron scattering technique invented by Mezei, which uses time reversal of the neutron spin evolution to measure energy loss in an inelastic neutron scattering process [2]. Photon polarization precession spectroscopy was proposed recently by Röhlsberger [3] for studies of spin waves that exhibit similarities to the neutron spin echo. Fung et al. proposed a space-domain analog of the echo spectroscopy for resonant inelastic soft x-ray scattering applications [4]. Defocusing and refocusing of the spectral components is achieved by angular dispersion from curved diffraction gratings. This approach has been recently demonstrated by Lai et al. [5].

Here, we propose a hard x-ray version of the echo spectroscopy, which can be applied for non-resonant and resonant high-resolution inelastic x-ray scattering applications. Diffraction gratings are not practical in the hard x-ray regime. However, as was demonstrated in [6, 7], the angular dispersion in the hard x-ray regime can be achieved by Bragg diffraction from asymmetrically cut crystals or from special arrangements of asymmetrically cut crystals [8, 9], which are a hard x-ray analog of the optical diffraction gratings and optical prisms. In the space-domain echo-spectrometer proposed here, an image of a point-like x-ray source is defocused by a dispersing system comprised of asymmetrically cut Bragg diffracting crystals. The defocused image is refocused into a point (echo) in a time-reversal dispersing system. We show, if the defocused beam is inelastically scattered from a sample, the echo signal acquires a spatial distribution, which is a map of the energy transfer spectrum in the scattering process. The spectral resolution of the echo spectroscopy does not rely on the monochromaticity of the x-rays, thus ensuring strong signals along with a very high spectral resolution.

In the present paper, we use an analytical ray-transfer matrix approach and the dynamical theory of x-ray diffraction in crystals to calculate and analyze the performance of a generic echo spectrometer comprised of defocusing and refocusing dispersing elements, to derive conditions for refocusing and expressions for the spectral resolution of the echo spectrometer. Specific designs of the hard x-ray echo spectrometers are introduced with a spectral resolution $\Delta\varepsilon = 0.1 - 0.02$ meV at photon energies $E \simeq 9.1$ keV and $E \simeq 4.6$ keV, comprised of defocusing and refocusing systems with multi-crystal in-line dispersing elements featuring both large cumulative dispersion rates $\mathcal{D}_{\cup} \gtrsim 25 - 60$ μrad/meV, transmission bandwidths $\Delta E_{\cup} \simeq 5 - 13$ meV, and a dynamical range $\Delta E_{\cup}/\Delta\varepsilon \simeq 100 - 500$.

We start here by considering optical systems featuring a combination of focusing and energy dispersing capabilities. We assume that such systems can, first, focus *monochromatic* x-rays from a source of a linear size Δx_0 in a source plane (reference plane 0 perpendicular to the optical axis z in Fig. 1) onto an intermediate image plane (reference plane 1 in Fig. 1) with an image linear size $\Delta x_1 = |A|\Delta x_0$, where A is a magnification factor of the optical system. In addition, the system can disperse photons in such a way that the location of the source image for photons with an energy $E + \delta E$ is displaced in the image plane by $G\delta E$ from the location of the image for photons with energy E. Here, G is a linear dispersion

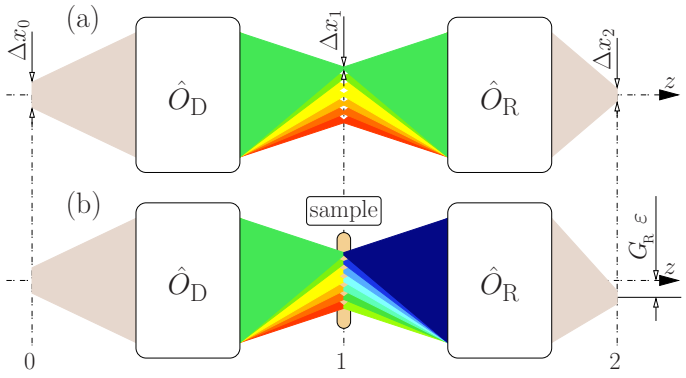

FIG. 1: Graphical presentation of the echo spectroscopy principles. (a) Photons from a source with a linear size Δx_0 in the reference source plane 0 are focused onto a spot Δx_1 in the intermediate image plane 1 by a focusing-dispersing system $\hat{O}_\mathrm{D}$. Each spectral component, indicated by different color, is focused at a different location due to dispersion in $\hat{O}_\mathrm{D}$. All spectral components of the x-rays are refocused by a consecutive time-reversal focusing-dispersing system $\hat{O}_\mathrm{R}$ onto the same spot Δx_2 (echo) in the image plane 2. (b) Inelastic x-ray scattering with an energy transfer ε (indicated by changed color) from a sample in the reference plane 1 results in a lateral shift $G_\mathrm{R}\varepsilon$ of the echo signal equal for all spectral components.

rate of the system. As a result, although monochromatic x-rays are focused, the whole spectrum of x-rays is defocused, due to linear dispersion.

We will use the ray-transfer matrix technique [10–12] to propagate paraxial x-rays through such optical systems and to determine linear and angular sizes of the x-ray beam along the optical axis. A paraxial ray in any reference plane is characterized by its distance x from the optical axis, by its angle ξ with respect to that axis, and the deviation δE of the photon energy from a nominal value E. The ray vector $\boldsymbol{r}_0 = (x_0, \xi_0, \delta E)$ at an input source plane is transformed to $\boldsymbol{r}_1 = (x_1, \xi_1, \delta E) = \hat{O}\boldsymbol{r}_0$ at the output reference plane (image plane), where $\hat{O} = \{ABG; CDF; 001\}$ is a ray-transfer matrix of an optical element placed between the planes. Only elastic processes in the optical systems are taken into account, that is reflected by zero and unity terms in the lowest row of the ray-transfer matrices.

Focusing of the monochromatic spectral components requires that matrix element $B = 0$. The ray-transfer matrix of any focusing-dispersing system in a general case therefore reads as

$$\hat{O} = \{A\,0\,G;\, CDF; 001\} \tag{1}$$

with A and G elements defined above. The system blurs the polychromatic source image, because of linear dispersion, as mentioned earlier and graphically presented in Fig. 1(a). However, another focusing-dispersing system can be used to refocus the source onto reference plane 2. Indeed, propagation of x-rays through the defocusing system $\hat{O}_\mathrm{D}$ and a second system, which we will refer to as a refocusing or time-reversal system $\hat{O}_\mathrm{R}$ (see Fig. 1) is given by a combined ray-transfer matrix

$$\hat{O}_\mathrm{C} = \hat{O}_\mathrm{R}\hat{O}_\mathrm{D} = \{A_\mathrm{C}\,0\,G_\mathrm{C}; C_\mathrm{C}D_\mathrm{C}F_\mathrm{C}; 001\}$$
$$= \begin{pmatrix} A_\mathrm{R}A_\mathrm{D} & 0 & A_\mathrm{R}G_\mathrm{D} + G_\mathrm{R} \\ C_\mathrm{R}A_\mathrm{D} + D_\mathrm{R}C_\mathrm{R} & D_\mathrm{R}D_\mathrm{D} & C_\mathrm{R}G_\mathrm{D} + D_\mathrm{R}F_\mathrm{D} + F_\mathrm{R} \\ 0 & 0 & 1 \end{pmatrix}, \tag{2}$$

and by a ray vector $\boldsymbol{r}_2 = (x_2, \xi_2, \delta E) = \hat{O}_\mathrm{C}\boldsymbol{r}_0$.

Here we arrive at a crucial point. If

$$G_\mathrm{C} = A_\mathrm{R}G_\mathrm{D} + G_\mathrm{R} = 0, \tag{3}$$

the linear dispersion at the exit of the combined system vanishes, because dispersion in the defocusing system is compensated (time reversed) by dispersion in the refocusing system. As a result, the combined system refocuses all photons independent of the photon energy to the same location, x_2 in image plane 2, to a spot with a linear size

$$\Delta x_2 = |A_\mathrm{R}A_\mathrm{D}|\Delta x_0 \equiv |A_\mathrm{R}|\Delta x_1, \tag{4}$$

as shown schematically in Fig. 1(a). Such behavior is an analog of the echo phenomena. Here, however, it takes place in space, rather than in the time domain.

Now, what happens if a sample is placed into the intermediate image plane 1, [Fig. 1(b)], which can scatter photons inelastically? In an inelastic scattering process, a photon with an arbitrary energy $E + \delta E$, changes its value to $E + \delta E + \varepsilon$. Here ε is an energy transfer in the inelastic scattering process. The ray vector $\boldsymbol{r}_1 = (x_1, \xi_1, \delta E)$ before scattering transforms to $\boldsymbol{r}'_1 = (x_1, \xi'_1, \delta E + \varepsilon)$ after inelastic scattering. Propagation of $\boldsymbol{r}'_1$ through the time-reversal system results in a ray vector $\boldsymbol{r}'_2 = (x'_2, \xi'_2, \delta E + \varepsilon) = \hat{O}_\mathrm{R}\boldsymbol{r}'_1$. Assuming that refocusing condition (3) holds, we come to a decisive point: all photons independent of the incident photon energy $E + \delta E$ are refocused to the same location

$$x'_2 = x_2 + G_\mathrm{R}\varepsilon, \qquad x_2 = A_\mathrm{R}A_\mathrm{D}x_o, \tag{5}$$

which is, however, shifted from x_2 by $G_\mathrm{R}\varepsilon$, a value proportional to the energy transfer ε in the inelastic scattering process. The essential point is that, the combined defocusing-refocusing system maps the inelastic scattering spectrum onto image plane 2. The image is independent of the spectral composition $E + \delta E$ of the photons in the incident beam.

The spectral resolution $\Delta\varepsilon$ of the echo spectrometer is calculated from the condition, that the shift due to inelastic scattering $x'_2 - x_2 = G_\mathrm{R}\varepsilon$ is at least as large as the linear size Δx_2 of the echo signal (4):

$$\Delta\varepsilon = \frac{\Delta x_2}{|G_\mathrm{R}|} \equiv \frac{|A_\mathrm{R}|\Delta x_1}{|G_\mathrm{R}|} \equiv \frac{|A_\mathrm{R}A_\mathrm{D}|\Delta x_o}{|G_\mathrm{R}|}. \tag{6}$$

Here it is assumed that the spatial resolution of the detector is better than Δx_2.

These results constitute the underlying principle of x-ray echo spectroscopy. Noteworthy, angular dispersion always results in an inclined intensity front, i.e., in dispersion both perpendicular to and along the beam propagation direction [13]. Therefore, x-rays are defocused and refocused also in the time domain, as in spin-echo. As a result, inelastic scattering spectra can be also mapped by measuring time distributions in the detector, given a short-pulse source.

Perfect refocusing takes place if the linear dispersion of the combined system $G_{\rm C} = A_{\rm R} G_{\rm D} + G_{\rm R}$ vanishes, as in Eq. (3). Refocusing can still take place with good accuracy if $|G_{\rm C}|$ is sufficiently small:

$$|G_{\rm C}| \Delta E_{\cup} \ll \Delta x_2 . \qquad (7)$$

Here $\Delta E_{\cup}$ is the bandwidth of x-rays in image plane 2. Tolerances on the echo spectrometer parameters and on the sample shape can be calculated with Eq. (7).

The above approach is general and applicable to any frequency domain. A particular version was proposed in the soft x-ray domain, with diffraction gratings as dispersing elements [4, 5].

Diffraction gratings are not practical in the hard x-ray regime. Extension into the hard x-ray regime is therefore nontrivial. In this regard, as was demonstrated in [6, 7], the angular dispersion in the hard x-ray regime can be achieved by Bragg diffraction from asymmetrically cut crystals, i.e., from crystals with the reflecting atomic planes not parallel to the entrance surface. This is a hard x-ray analog of the optical diffraction gratings or optical prisms. A large dispersion rate is a key for achieving high spectral resolution in angular-dispersive x-ray spectrometers [9, 14], including echo spectrometers, see Eq. (6). This is achieved, first, by using strongly asymmetric Bragg reflections close to backscattering [6, 7], and, second, by enhancing the single-reflection dispersion rate considerably by subsequent asymmetric Bragg reflections from crystals in special arrangements [8] exemplified below. In the following two steps, we will show how the principle scheme of a generic echo spectrometer presented above, can be realized in the hard x-ray regime by using multi-crystal arrangements as dispersing elements.

In the first step, we propose a principle optical scheme of a hard x-ray echo spectrometer (Fig. 2) comprised of the defocusing $\hat{O}_{\rm D}$ and refocusing $\hat{O}_{\rm R}$ dispersing systems. The x-ray source is in reference plane 0, the sample is in plane 1, and the position-sensitive detector is in plane 2. The defocusing system $\hat{O}_{\rm D}$ is proposed here as a combination of a Bragg (multi)crystal dispersing element $\rm D_D$ and a focusing element f. As has been shown in [9], such a system can be represented by a ray-transfer matrix (1) with the magnification $A_{\rm D}$ and linear dispersion $G_{\rm D}$ matrix elements given by

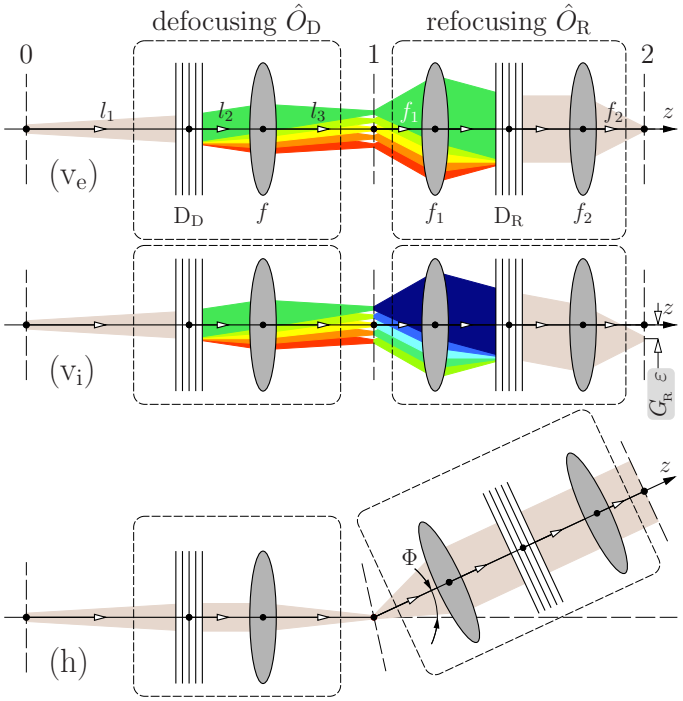

FIG. 2: Optical scheme of an x-ray echo spectrometer, comprised of the defocusing $\hat{O}_{\rm D}$ and refocusing $\hat{O}_{\rm R}$ dispersing systems; the x-ray source in reference plane 0; the sample in 1; and the position-sensitive detector in 2. The spectrometer is shown in the vertical dispersion plane for elastic ($\rm v_e$) and inelastic ($\rm v_i$) scattering, and in the horizontal scattering plane (h) with the refocusing system at a scattering angle Φ. See text for details.

$$A_{\rm D} = -\frac{1}{b_{\cup_D}} \frac{l_3}{l_{12}}, \quad G_{\rm D} = \mathcal{D}_{\cup_D} \frac{l_3 l_1}{b_{\cup_D}^2 l_{12}}, \quad l_{12} = \frac{l_1}{b_{\cup_D}^2} + l_2 . \qquad (8)$$

Here, l_1, l_2, and l_3, are the distances between the x-ray source, the dispersing element $\rm D_D$, the focusing element f with focal length $f = (l_{12}^{-1} + l_3^{-1})^{-1}$, and the sample in the image plane 1, respectively (Fig. 2). The dispersing (multi)crystal system $\rm D_D$ is characterized by the cumulative angular dispersion rate $\mathcal{D}_{\cup_D}$, and cumulative asymmetry factor $b_{\cup_D}$, which are defined in [9] (see also supplemental material [17]).

For the spectrometer to feature a large throughput, the refocusing system $\hat{O}_{\rm R}$ has to be capable of collecting x-ray photons in a large solid angle scattered from the sample. For this purpose, we propose using a hard x-ray focusing-dispersing system of a spectrograph-type considered in [9], and schematically shown in Fig 2. A collimating element f_1 collects photons in a large solid angle and makes x-ray beams of each spectral component parallel. The collimated beam impinges upon the Bragg (multi)crystal dispersing element $\rm D_R$ with the cumulative angular dispersion rate $\mathcal{D}_{\cup_R}$, and the cumulative asymmetry factor $b_{\cup_R}$. The focusing element f_2 focuses x-rays

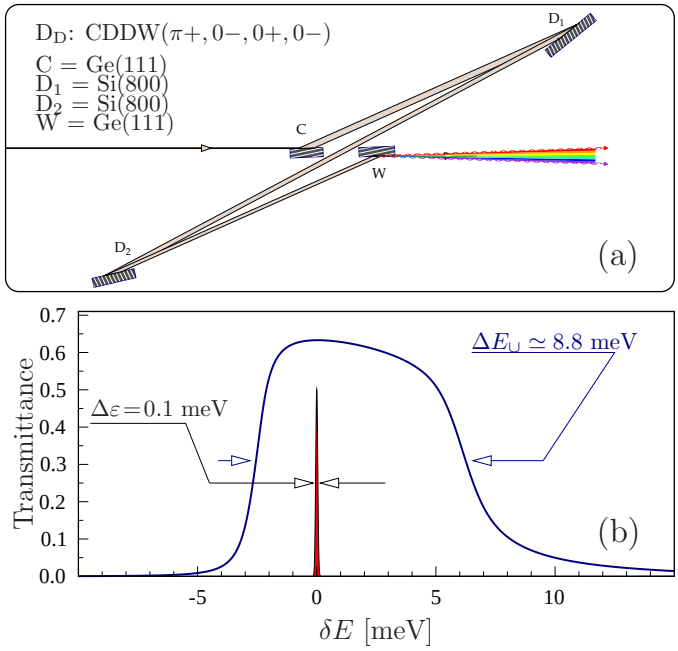

FIG. 3: Dispersing element D_D (a) of the defocusing system $\hat{O}_D$ (see Fig. 2) and its spectral transmittance function (b). D_D is an example of an in-line four-crystal CDDW-type dispersing optic, comprised of collimating (C), dispersing (D_1, D_2), and wavelength-selecting (W) crystals in a (π+,0−,0+,0−) scattering configuration. With the crystal parameters provided in the supplemental material [17], the dispersing element D_D features a spectral transmission function with a $\Delta E_\cup = 8.8$ meV bandwidth (b), a cumulative angular dispersion rate $\mathcal{D}_{\cup_D} = -25$ μrad/meV, and a cumulative asymmetry factor $b_{\cup_D} = 1.4$. The sharp line in (b) presents the 0.1-meV spectral resolution of an x-ray echo spectrometer, designed for use with 9.1-keV photons.

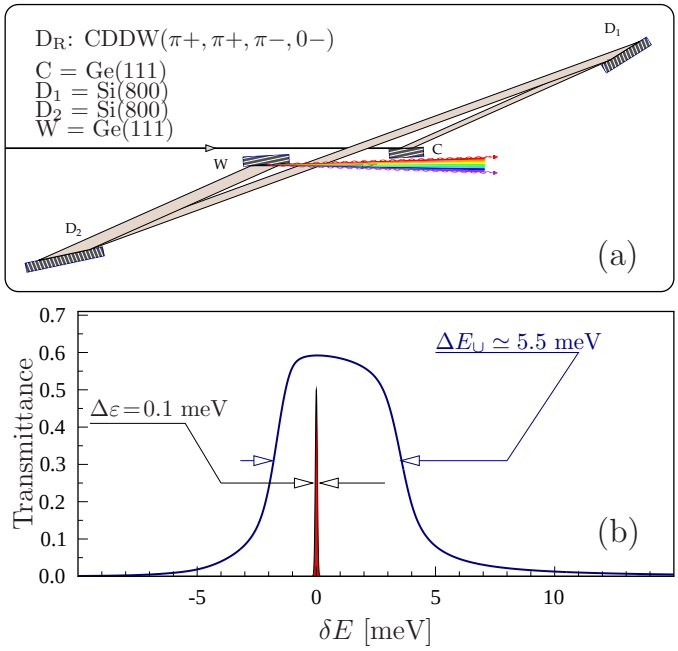

FIG. 4: Dispersing element D_R (a) of the refocusing system $\hat{O}_R$ (see Fig. 2) and its spectral transmittance function (b). Similar to D_D in Fig. 3, D_R is an example of the in-line four-crystal CDDW-type dispersing optic, but, in a (π+,π+,π−,0−) scattering configuration. With the crystal parameters provided in [17], the dispersing element D_D features a spectral transmission function with a $\Delta E_\cup = 5.5$ meV bandwidth (b), a cumulative angular dispersion rate $\mathcal{D}_{\cup_D} = -43$ μrad/meV, a cumulative asymmetry factor $b_{\cup_D} = 0.36$, and $\mathcal{D}_{\cup_D}/b_{\cup_D} = -120$ μrad/meV.

in the vertical dispersion plane onto the position-sensitive detector in the image plane 2. As shown in [9] (see also supplemental material [17]) such a system is described by a ray-transfer matrix (1) with the magnification A_R and linear dispersion G_R matrix elements given by

$$A_R = -\frac{b_{\cup_R} f_2}{f_1}, \qquad G_R = \mathcal{D}_{\cup_R} f_2. \tag{9}$$

Using Eqs. (3), (8), and (9) we obtain for the refocusing condition in the hard x-ray echo spectrometer

$$\frac{l_3 l_1}{l_1 + b^2_{\cup_D} l_2} \mathcal{D}_{\cup_D} = f_1 \frac{\mathcal{D}_{\cup_R}}{b_{\cup_R}}. \tag{10}$$

For the spectral resolution $\Delta\varepsilon$ of a hard x-ray echo spectrometer we obtain from Eqs. (6), (8), and (9):

$$\Delta\varepsilon = \frac{|b_{\cup_R}|}{|\mathcal{D}_{\cup_R}|} \frac{\Delta x_1}{f_1}. \tag{11}$$

As follows from Eq. (11), the spectral resolution of the echo spectrometer is determined solely by the parameters of the refocusing system, i.e., by the resolution of the hard x-ray spectrograph [9]. The parameters of the defocusing system determine only the size of the secondary monochromatic source on the sample $\Delta x_1 = |A_D| \Delta x_0$.

In the second step, we consider the particular optical designs of x-ray echo spectrometers with a very high spectral resolution $\Delta\varepsilon \lesssim 0.1$ meV. For practical reasons, we will assume that the secondary *monochromatic* source size is $\Delta x_1 \simeq 5$ μm, and the focal length is $f_1 \simeq 0.4$ m of the collimating element in the refocusing system. Then, Eq. (11) requires the ratio $|\mathcal{D}_{\cup_R}|/|b_{\cup_R}| \simeq 125$ μrad/meV for the dispersive element D_R. Assuming the distance $l_3 \simeq 2$ m from the focusing element to the sample in the defocusing system, and $l_1 \gg b^2_{\cup_D} l_2$, we estimate from Eq. (10) for the required cumulative dispersing rate $|\mathcal{D}_{\cup_R}| \simeq 25$ μrad/meV in the defocusing dispersive element. These are relatively large values. Typically, in a single Bragg reflection, a maximum dispersion rate is $\mathcal{D} \simeq 6-8$ μrad/meV for photons with energy $E \simeq 10$ keV [7, 15]. As mentioned before, multi-crystal arrangements can be used to enhance the dispersion rate [8].

Such large dispersion rates $\mathcal{D}_\cup$, unfortunately, tend to decrease the transmission bandwidths $\Delta E_\cup$ of the dispersing elements [8, 9]. Achieving strong signals in IXS

experiments, however, requires $\Delta E_{\cup} \gg \Delta\varepsilon$. Therefore, optical designs of the dispersing elements have to be found featuring both large $\mathcal{D}_{\cup}$ and $\Delta E_{\cup}$. Figures 3 and 4 show representative examples of multi-crystal CDDW-type inline dispersing elements [14–16] of the defocusing and refocusing systems, respectively, with the required cumulative dispersion rates, asymmetry factors, and with bandwidths $\Delta E_{\cup} \simeq 5.5-9$ meV, i.e., $\Delta E_{\cup}/\Delta\varepsilon \simeq 55-90$, designed for use with 9.1-keV photons.

The CDDW optic in the (π+,0−,0+,0−) scattering configuration is preferred for the defocusing dispersing element D_{D} (Fig. 3) as it provides the required dispersion rate $|\mathcal{D}_{\cup_D}| \simeq 25$ μrad/meV, significant transmission bandwidth $\Delta E_{\cup} \simeq 9$ meV, and is compact. The CDDW optic in the (π+,π+,π−,0−) configuration is better suited for the refocusing dispersing element D_{R} (Fig. 4). It provides the large ratio $|\mathcal{D}_{\cup_R}|/|b_{\cup_R}| \simeq 120$ μrad/meV required for the high spectral resolution [see Eq. (11)] and substantial transmission bandwidth $\Delta E_{\cup} \simeq 5.5$ meV, although smaller than in the D_{D}-case.

The total beam size on the sample is $\simeq G_{\mathrm{D}} \Delta E_{\cup}$. For the spectrometer exemplified here, it is estimated to be $\simeq 275$ μm. Equation (7) together with Eqs. (8) and (9) can be used to estimate tolerances on the admissible variations of the focal distances, sample displacement, sample surface imperfections, etc. As discussed in the supplemental material [17], the tolerances are in a millimeter range in the case of the 0.1-meV spectrometer.

Details on the optical designs and examples of the dispersing elements designed for use with a lower photon energy of 4.57 keV and larger $\Delta E_{\cup} \simeq 13-10$ meV, can be found in the supplemental material [17]. All these examples showcase the applicability of echo spectroscopy in a wide spectral range, and its feasibility both with synchrotron radiation and x-ray free electron laser sources.

The point is that even higher spectral resolution $\Delta\varepsilon \lesssim 0.02$ meV can be achieved with x-ray echo spectrometers by increasing the dispersion rates $\mathcal{D}_{\cup}$ in the dispersing elements. This, however, will result in their narrower transmission bandwidths $\Delta E_{\cup}$. Still, an approximately constant ratio $\Delta E_{\cup}/\Delta\varepsilon$ holds. Alternatively, the spectral resolution can be improved by increasing the focal length f_1 in the refocusing system, see Eq. (11).

The essential feature of the echo spectrometers is that the signal strength, which is proportional to the product of the bandwidths of the photons on the sample and on the detector, is enhanced by $(\Delta E_{\cup}/\Delta\varepsilon)^2 \simeq 10^3 - 10^4$ compared to what is possible with the standard scanning-IXS-spectrometer approach.

In conclusion, x-ray echo spectroscopy, a counterpart of neutron spin-echo, is introduced here to overcome limitations in spectral resolution and weak signals of the traditional inelastic hard x-ray scattering (IXS) probes. Operational principles, refocusing conditions, and spectral resolutions of echo spectrometers are substantiated by an analytical ray-transfer-matrix approach. A principle optical scheme for a hard x-ray echo spectrometer is proposed with multi-crystal arrangements as dispersing elements. Concrete schemes are discussed with 5–13-meV transmission bandwidths, a spectral resolution of 0.1-meV (extension to 0.02-meV is realistic), and designed for use with 9.1-keV and 4.6-keV photons. The signal in echo spectrometers is enhanced by at least three orders of magnitude compared to what is possible with the standard scanning-IXS-spectrometer approach.

X-ray echo spectrometers require a combination of the CDDW dispersing elements and focusing optics as major optical components. Such components have been experimentally demonstrated recently [8, 14]. Implementation of x-ray echo spectrometers is, therefore, realistic.

Stimulating discussions with D.-J. Huang (NSRRC) are greatly appreciated. S.P. Collins (DLS) is acknowledged for reading the manuscript and for valuable suggestions. Work at Argonne National Laboratory was supported by the U.S. Department of Energy, Office of Science, under Contract No. DE-AC02-06CH11357.

* Electronic address: shvydko@aps.anl.gov

[1] E. L. Hahn, Phys. Rev. **80**, 580 (1950).
[2] F. Mezei, ed., *Neutron Spin Echo.*, vol. 128 of *Lecture Notes in Physics* (Springer, Berlin, 1980).
[3] R. Röhlsberger, Phys. Rev. Lett. **112**, 117205 (2014).
[4] H. S. Fung, C. T. Chen, L. J. Huang, C. H. Chang, S. C. Chung, D. J. Wang, T. C. Tseng, and K. L. Tsang, AIP Conf. Proc. **705**, 655 (2004).
[5] C. H. Lai, H. S. Fung, W. B. Wu, H. Y. Huang, H. W. Fu, S. W. Lin, S. W. Huang, C. C. Chiu, D. J. Wang, L. J. Huang, et al., Journal of Synchrotron Radiation **21**, 325 (2014).
[6] Yu. Shvyd'ko, *X-Ray Optics – High-Energy-Resolution Applications*, vol. 98 of *Optical Sciences* (Springer, Berlin Heidelberg New York, 2004).
[7] Yu. V. Shvyd'ko, M. Lerche, U. Kuetgens, H. D. Rüter, A. Alatas, and J. Zhao, Phys. Rev. Lett. **97**, 235502 (2006).
[8] Yu. Shvyd'ko, S. Stoupin, K. Mundboth, and J. Kim, Phys. Rev. A **87**, 043835 (2013).
[9] Yu. Shvyd'ko, Phys. Rev. A **91**, 053817 (2015).
[10] H. Kogelnik and T. Li, Appl. Opt. **5**, 1550 (1966).
[11] T. Matsushita and U. Kaminaga, Journal of Applied Crystallography **13**, 472 (1980).
[12] A. E. Siegman, *Lasers* (University Science Books, Sausalito, California, 1986).
[13] Yu. Shvyd'ko and R. Lindberg, Phys. Rev. ST Accel. Beams **15**, 100702 (2012).
[14] Yu. Shvyd'ko, S. Stoupin, D. Shu, S. P. Collins, K. Mundboth, J. Sutter, and M. Tolkiehn, Nature Communications **5:4219** (2014).
[15] Yu. Shvyd'ko, S. Stoupin, D. Shu, and R. Khachatryan, Phys. Rev. A **84**, 053823 (2011).
[16] S. Stoupin, Yu. V. Shvyd'ko, D. Shu, V. D. Blank, S. A. Terentyev, S. N. Polyakov, M. S. Kuznetsov, I. Lemesh, K. Mundboth, S. P. Collins, et al., Opt. Express **21**, 30932 (2013).

[17] See Supplemental Material http://link.aps.org/ supplemental/??.??/PhysRevLett.116.???, which includes Refs. [18-22], for details on the ray-transfer matrices of the defocusing and refocusing systems, on the optical design and crystal parameters of the CDDW dispersing elements operating at 9.13-keV and 4.57-keV photon energies, on the focusing and collimating optics, on the echo spectrometer tolerances discussed in the Letter.

[18] N. Hodgson and H. Weber, *Laser Resonators and Beam Propagation: Fundamentals, Advanced Concepts and Applications*, Optical Sciences (Springer, Berlin Heidelberg New York, 2005).

[19] T. Matsushita and U. Kaminaga, Journal of Applied Crystallography **13**, 465 (1980).

[20] A. Snigirev, V. Kohn, I. Snigireva, and B. Lengeler, Nature **384**, 49 (1996).

[21] B. Lengeler, C. Schroer, J. Tümmler, B. Benner, M. Richwin, A. Snigirev, I. Snigireva, and M. Drakopoulos, J. Synchrotron Radiation **6**, 1153 (1999).

[22] K. Mundboth, J. Sutter, D. Laundy, S. Collins, S. Stoupin, and Yu. Shvydko, J. Synchrotron Radiation **21**, 16 (2014).